

# Limits on the radiative decay of sterile neutrino dark matter from the unresolved cosmic and soft x-ray backgrounds

Kevork N. Abazajian,<sup>1,2</sup> Maxim Markevitch,<sup>3,4</sup> Savvas M. Koushiappas,<sup>2,5</sup> and Ryan C. Hickox<sup>3</sup>

<sup>1</sup>*Department of Physics, University of Maryland, College Park, Maryland 20742, USA*

<sup>2</sup>*Theoretical Division, Los Alamos National Laboratory, Los Alamos, New Mexico 87545, USA*

<sup>3</sup>*Harvard-Smithsonian Center for Astrophysics, 60 Garden Street, Cambridge, Massachusetts 02138, USA*

<sup>4</sup>*Space Research Institute, Russian Acad. Sci., Profsoyuznaya 84/32, Moscow 117997, Russia*

<sup>5</sup>*ISR Division, Los Alamos National Laboratory, Los Alamos, New Mexico 87545, USA*

(Received 7 November 2006; published 20 March 2007)

We present upper limits on line emission in the Cosmic X-ray background (CXB) that would be produced by decay of sterile neutrino dark matter. We employ the spectra of the unresolved component of the CXB in the *Chandra* Deep Fields North and South obtained with the *Chandra* CCD detector in the  $E = 0.8\text{--}9$  keV band. The expected decay flux comes from the dark matter on the lines of sight through the Milky Way galactic halo. Our constraints on the sterile neutrino decay rate are sensitive to the modeling of the Milky Way halo. The highest halo mass estimates provide a limit on the sterile neutrino mass of  $m_s < 2.9$  keV in the Dodelson-Widrow production model, while the lowest halo mass estimates provide the conservative limit of  $m_s < 5.7$  keV ( $2\sigma$ ). We also discuss constraints from a short observation of the softer ( $E < 1$  keV) X-ray background with a rocket-borne calorimeter by McCammon and collaborators.

DOI: [10.1103/PhysRevD.75.063511](https://doi.org/10.1103/PhysRevD.75.063511)

PACS numbers: 95.35.+d, 14.60.Pq, 14.60.St, 98.65.-r

## I. INTRODUCTION

The abundance of cosmological dark matter is now well quantified by cosmological observations to better than 10% in density [1,2], yet its identity remains unknown. Several indicators point towards a modification of the properties of dark matter clustering from the cold dark matter (CDM) paradigm to resolve potential discrepancies that persist with the ansatz of an absolutely *cold* dark matter candidate. Among potential problems with CDM are indications for density cores in local group dwarf spheroidal galaxies [3–6] and the lack of a correspondence of the observed dwarf galaxies with the number of halos expected with the same maximal velocity dispersion or mass [7,8]. This has prompted the investigation of alternatives to CDM, such as warm dark matter (WDM) [9,10], late-decaying superWIMP dark matter [11,12], fuzzy cold dark matter [13], or meta-CDM [14].

A leading particle candidate for WDM is a fermion that has no standard model interactions, yet couples with the standard model neutrino sector via the neutrino mass generation mechanism, namely, a sterile neutrino. Extensions to the standard model of particle physics typically include sterile neutrinos, including left-right symmetric (mirror) models [15], supersymmetric axinos as sterile neutrinos [16], superstring models [17], models with large extra dimensions [18,19], and phenomenological models such as the  $\nu$ MSM [20]. Other motivations for a sterile neutrino to have parameters in the parameter space of interest for their oscillation production as dark matter are the generation of pulsar kicks [21–23], Type II supernova shock heating enhancement [24], and enhanced molecular hydrogen formation at high redshift [25].

Sterile neutrinos may be produced in the early universe via nonresonant Dodelson-Widrow (DW) oscillation production [26], or via a resonant oscillation production in cosmologies with a nonzero lepton number [27]. Both nonresonant DW and resonant production models fall in a parameter space that is continuous in the cosmological lepton number, with non-negligible lepton numbers allowing for resonant production at smaller mixing angles. The DW model is the simplest model for sterile neutrino dark matter production, because it assumes a standard thermal history in the early universe, zero lepton numbers, and no additional couplings of the sterile neutrino. For the nonresonant and resonant cases, production occurs near the quark-hadron transition, and the relation between the critical density in sterile neutrinos and its mixing parameters with active neutrinos is given by Refs. [28–30]. Sterile neutrinos can be produced at smaller mixing angles than the DW mechanism through the resonant production model or via additional couplings to other particles, such as the inflaton [31]. They could be produced at larger mixing angles than the DW model if over-abundance due to the nonresonant oscillation production is avoided through dilution by massive particle decay after production [32] or by a low reheating temperature scale in the early universe [33].

A particularly interesting particle-mass range for the sterile neutrino can be framed by the mass required to produce a constant density core of 100–300 pc like that discussed for the Fornax dwarf spheroidal [3,4], which is 0.5–1.3 keV [5,34], or more massive if the phase-space packing limit is not achieved. In addition, the requirement for a viable sterile neutrino dark matter candidate constrains their parameter space by demanding that: (i) the

total decay time-scale is larger than the age of the universe, (ii) it is consistent with radiation energy density constraints from primordial nucleosynthesis and the cosmic microwave background, (iii) it is consistent with lithium photo-production constraints, and (iv) it is consistent with the diffuse X-ray background, and X-ray observations of clusters or other nearby structures [35–37]. Sterile neutrinos are constrained by X-ray observations because of the considerable radiative decay width to a photon and lighter-mass neutrino due to the same coupling required for their production, producing a spectral line in the X-ray [38].

Abazajian, Fuller and Tucker [35] found that X-ray observations could present the most stringent constraints in the upper particle-mass range regions of parameter space. An estimate in that work of the sensitivities of X-ray observations of the large dark matter overdensities present in clusters of galaxies and field galaxies was made and led to an estimated limit from *XMM-Newton* observations of the Virgo cluster on the nonresonant DW production model on the particle mass of the sterile neutrino. Recent work has shown that the local radiative decay flux from dark matter overdensities in Local Group structures can be comparable to that estimated from clusters of galaxies and field galaxies, with reduced continuum emission and bigger angular size, and therefore increased sensitivity [39]. This was also found in subsequent observational work [40–42]. For example, using a nondetection of the decay line from the Andromeda galaxy by *XMM-Newton*, Watson *et al.* [40] derived  $m_s < 3.5$  keV in the DW model (95% CL).

Upper mass constraints from the lack of X-ray line flux are complementary to lower mass constraints from observed cosmological structure. Since sterile neutrinos behave as increasingly warm dark matter for lighter particle masses, observations of the lack of deviations from absolute cold dark matter clustering constrain lighter particle masses. Two recent analyses of a single measurement of the flux power spectrum of the Ly $\alpha$  forest from the Sloan Digital Sky Survey (SDSS) [43] find roughly similar constraints  $m_s > 14$  keV [44] and  $m_s \gtrsim 9$  keV [45]<sup>1</sup> in the DW model. These improved considerably relative to previous constraints at  $m_s \gtrsim 2$  keV, which used the inferred linear matter power spectrum from the SDSS and higher-resolution Ly $\alpha$  flux power spectra [46,47]. The improvement by a factor of 5 stems from the high-redshift ( $z \sim 4$ ) Ly $\alpha$  flux power spectra of the SDSS, where there is less enhancement of the amplitude of matter power at small scales due to the nonlinear growth of structure. The newer Ly $\alpha$  limits are quite stringent. When combined with X-ray observations of Andromeda and other mass halos, they would exclude the DW production mechanism for sterile

neutrinos. However, it should be noted that the amplitude and slope of the dark matter power spectrum inferred from the flux power spectrum measurement of Ref. [43] used in both sterile neutrino analyses is inconsistent with that inferred from the Wilkinson Microwave Anisotropy Probe (WMAP) third year data [1] and also indicates a number of relativistic degrees of freedom of  $N_\nu = 5.4^{+0.4}_{-0.6}$  [48], which is in tension both with that expected  $N_\nu = 3.046$  [49] for the case of active neutrinos alone and that constrained by primordial nucleosynthesis,  $N_\nu = 3.08^{+0.74}_{-0.68}$  [50]. This may indicate hidden systematic effects within the measurement presented in Ref. [43] of the Ly $\alpha$  flux power spectrum which could alleviate or remove constraints on the inferred matter power spectrum from the Ly $\alpha$  forest [51].

In this paper, we use *Chandra* spectra of the unresolved component of the Cosmic X-ray Background (CXB) in the direction of *Chandra* Deep Fields North and South (hereafter CDFN and CDFS) [52,53] to search for the contribution from the radiative decay of a sterile neutrino which could comprise the dark matter halo of the Milky Way (MW). In addition, we consider the sensitivity of an existing short measurement at lower energies (0.4–1 keV) with an X-ray calorimeter [54] to the sterile neutrino signal.

## II. THE DARK MATTER MODEL

For a sterile neutrino of mass  $m_s$  and a mixing angle  $\theta$ , the decay rate for a Dirac-type active-sterile mass coupling is given by [38,55]

$$\Gamma_\gamma(m_s, \theta) = 1.36 \times 10^{-29} \text{ s}^{-1} \left( \frac{\sin^2 2\theta}{10^{-7}} \right) \left( \frac{m_s}{1 \text{ keV}} \right)^5. \quad (1)$$

Note that here we identify the particle mass  $m_s$  with that of the mass eigenstate most closely associated with the sterile neutrino. The dominantly sterile neutrino mass eigenstate decays into a photon of  $E = m_s/2$  and a predominantly active neutrino mass eigenstate. The decay rate as a function of particle mass, for a ratio of dark matter density to critical density  $\Omega_s$  and a fixed quark-hadron transition temperature is given by

$$\Gamma_\gamma^{\text{DW}}(m_s) = 9.95 \times 10^{-30} \text{ s}^{-1} \left( \frac{m_s}{1 \text{ keV}} \right)^{3.37} \left( \frac{\Omega_s}{0.26} \right). \quad (2)$$

Here, we use the inferred relation between mass and mixing angle which is necessary to produce the appropriate cosmological density of dark matter in sterile neutrinos through the DW mechanism [28]. We assume a crossover transition for the quark-hadron at a temperature of 170 MeV for the relation, Eq. (2). In general, this can vary significantly due to uncertainties in the nature of the quark-hadron transition, as pointed out in Abazajian and Fuller [29] and shown in greater detail recently by Asaka, Laine and Shaposhnikov [56].

The expected flux from the decay of sterile neutrino dark matter depends on the mass of the particle, its decay rate, as

<sup>1</sup>We have applied a rough 10% reduction in the limit of Ref. [45] in order to include relevant nonthermal effects, though this correction is significantly mass dependent [28].

well as the distance and distribution of dark matter across the field of view of a detector, such as *Chandra*. Estimates of the dark matter mass within the field of view of the detector come from dynamic measures of the galactic mass profiles, or for clusters of galaxies, from the X-ray hydrostatic method or gravitational lensing.

The flux in the neutrino decay line reaching the detector is calculated as follows. Denoting  $x$  the linear coordinate along the line of sight and  $d\Omega$  an element of the detector field of view (FOV), each corresponding volume element  $x^2 d\Omega dx$  contains  $\rho_{\text{dm}}(x)/m_s$  neutrinos, each decaying with a frequency  $\Gamma_\gamma$  given by Eqs. (1) and (2). In Euclidean geometry (i.e., as long as the object redshift  $z$  satisfies  $(1+z)^4 \approx 1$ ), the photon flux from this volume element reaching a unit effective area of the detector is

$$df = x^2 d\Omega dx \frac{\Gamma_\gamma \rho_{\text{dm}}(x)}{m_s} \frac{1}{4\pi x^2}. \quad (3)$$

The flux from the cone subtended by the detector FOV (in photons  $\text{s}^{-1} \text{cm}^{-2}$ ) is therefore

$$f = \frac{\Gamma_\gamma}{4\pi m_s} \int d\Omega \int \rho_{\text{dm}}(x) dx = \frac{\Gamma_\gamma}{4\pi m_s} \Omega \bar{S}_{\text{dm}}, \quad (4)$$

where the first integral is over the FOV and the second integral is along the line of sight, and  $\bar{S}_{\text{dm}}$  is the dark matter mass column density averaged over the FOV  $\Omega$ . The flux coming from each direction in the FOV depends only on  $S_{\text{dm}}$  in that direction; details of the line of sight mass distribution, and even the distance to the object, are not important for objects at low  $z$ . For *Chandra*'s small FOV (a  $r = 5'$  circle used in this work), we can ignore the changes of the Milky Way mass column density across the FOV. However, in Sec. IV we will consider an instrument with a much wider FOV, for which we directly integrate the column density within the FOV.

To calculate  $S_{\text{dm}}$  for the Milky Way halo in the directions of the two *Chandra* CXB observations, we use mass models from Galactic dynamics measures presented in Klypin *et al.* [57] and Battaglia *et al.* [58], which are both consistent with each other and with Ref. [59]. We use the Navarro-Frenk-White (NFW) profile [60]

$$\rho(r) = \rho_s \left(\frac{r}{r_s}\right)^{-1} \left(1 + \frac{r}{r_s}\right)^{-2}, \quad (5)$$

where  $\rho_s$  is the characteristic density and  $r_s$  is the scale radius. The NFW profile is expected for CDM and should be consistent with WDM models where cores are expected to be much smaller than the MW NFW scale radius [61].

The dynamical constraints on the dark matter halo of the MW are complicated by the fact that we sit within this galaxy, and depend strongly on the measured orbital velocities of satellite dwarf galaxies. The 68% confidence region of the NFW models from Battaglia *et al.* also covers the allowed model range from Klypin *et al.*, while still being consistent with observations. We thus adopt that

interval for our estimates. These models have  $M_{\text{vir}} = 0.6 \times 10^{12} M_\odot$  (low mass MW) and  $M_{\text{vir}} = 2.0 \times 10^{12} M_\odot$  (high mass MW),  $R_{\text{vir}} = 255$  kpc,  $R_{\text{vir}}/r_s = 18$ , and  $R_\odot = 8$  kpc. In both models, most of the baryonic mass is concentrated in the central region of the MW (disk and bulge), which our lines of sight miss, thus we can simply (and somewhat conservatively) multiply the total density with the universal dark matter fraction  $f_{\text{DM}} = \Omega_{\text{DM}}/(\Omega_{\text{DM}} + \Omega_b) \approx 0.867$ , where the fraction of critical density of the dark matter we take is  $\Omega_{\text{DM}} = 0.26$ , and baryon density  $\Omega_b = 0.04$ . The uncertainties in the MW halo model are much larger than that of the universal dark matter fraction, which we keep fixed.

For a point at a distance  $x$  from the Sun along the line of sight with Galactic coordinates  $(\ell, b)$ , the distance from the center of the halo is

$$r = (x^2 - 2xR_\odot \cos b \cos \ell + R_\odot^2)^{1/2}, \quad (6)$$

which is used to evaluate the column density integral in Eq. (4). In the direction of the CDFN at  $\ell = 125.89^\circ$ ,  $b = 54.83^\circ$ , the dark matter surface density is

$$S_{\text{dm}} = \begin{cases} 0.0362 \text{ g cm}^{-2} & \text{(high mass MW)} \\ 0.0109 \text{ g cm}^{-2} & \text{(low mass MW)}. \end{cases} \quad (7)$$

For the CDFS at  $\ell = 223.57^\circ$ ,  $b = -54.44^\circ$ , the corresponding surface densities are 4% lower.

We integrated the MW halo out to  $R_{\text{vir}}$ . However, most of the column density accumulates at small radii (within  $0.1R_{\text{vir}}$ ), so the outer radial cutoff does not matter. It also means that the column density depends on small-scale deviations from the symmetric model. Therefore, our range of dark matter column densities is only qualitative and does not reflect the full uncertainty, which is difficult to quantify, and therefore we leave our inferred limits as they are but with the caveat of potentially non-negligible systematic uncertainty. A substantive measure of the systematic uncertainty may be estimated via comparisons with other independent measurements.

As a comparison, the mass surface density within  $5^\circ$  of the Galactic center is an order of magnitude higher, as is the surface density on the line of sight near the center of M31. Massive galaxy clusters have column densities of  $0.1\text{--}0.3 \text{ g cm}^{-2}$  in their core regions. Clearly, our lines of sight are not optimal for the neutrino line search, and more sensitive limits can be obtained, for example, from observations of the Galactic Center (which we will attempt in a future work). At the same time, our CDF datasets have the advantage of an almost complete removal of the sources causing the CXB and a very accurate background modeling.

### III. CHANDRA CXB SPECTRUM

The *Chandra X-ray Observatory* [62] has a 1 arcsecond on-axis angular resolution and is uniquely suited for resolving the CXB covered by its ACIS detector, which

operates in the 0.4–10 keV energy band. It has performed a series of very deep observations of two fields, CDFN and CDFS, for a total exposure of 2 Ms and 1 Ms, respectively, aimed at resolving as much of the extragalactic CXB into point sources as possible [63,64]. Hickox and Markevitch [52] (hereafter H06) have used these observations, along with recent accurate calibration of the ACIS internal background, to derive a spectrum of the CXB that is still unresolved after spatially excising all X-ray sources detectable in these deep exposures. They found that about 20% of the CXB in the 1–2 and 2–8 keV bands remains unresolved, while at  $E \lesssim 1$  keV, the Galaxy contributes a dominant genuinely diffuse component. The 1–8 keV unresolved spectrum is well modeled by a power law with a photon index  $\Gamma \approx 1.5$ , and the Galactic diffuse component by thermal emission from a  $T \approx 0.2$  keV plasma.

These unresolved spectra do not exhibit any emission lines that can be attributed to decaying sterile neutrinos in the Galactic halo, and we will use this fact to place upper limits on the neutrino line in the  $E = 0.8$ –8 keV range. We note that in a later work, Hickox and Markevitch [53] have additionally excised sources not detected in X-rays but seen by the *Hubble* Space Telescope in the optical. These sources collectively account for most of the unresolved 1–8 keV flux, with a residual CXB brightness consistent with zero. Although this seems advantageous for our upper limits, we will not use these new spectra, because excising those optical sources reduced the solid angle from which the CXB spectra are collected by a factor of 3, compared to that in H06. This increased statistical uncertainty and removed any advantage for our analysis. The CXB in either case is a small fraction of the detector background, and our constraints on the neutrino line are limited by photon statistics of this background. We thus elected to tolerate some unresolved CXB flux (modeled with a power law as described below) but have a significantly smaller statistical scatter in each spectral bin. At the same time, we will take advantage of a longer calibration exposure of the ACIS internal background that was used in the latter work.

Full account of the CDF spectra derivation is given in H06, and here we give only the relevant details. The CDFN dataset is divided into two, one observed with ACIS in FAINT mode and another in VFaint (the latter more advantageous for background modeling). We treat these subsets as independent observations (CDFN-F and CDFN-VF). After excluding periods of elevated detector background, their exposures are 472 ks and 537 ks, respectively. The CDFS was observed in FAINT mode and has a clean exposure of 568 ks. Solid angles, after the source exclusion, subtended by the CDFN and CDFS fields are  $0.0135 \text{ deg}^2$  and  $0.0159 \text{ deg}^2$ , respectively. The internal detector background is modeled and subtracted using a set of calibration observations in which ACIS was shielded from the sky. We will use a more recent 325 ks calibration dataset from Hickox and Markevitch [53], compared to

236 ks in H06. This exposure is still shorter than any of the CDF exposures, and the statistical uncertainty of this calibration spectrum will be the main limiting factor for our analysis. Otherwise, the CXB spectra that we analyze here are identical to those in H06.

As noted in H06, the three unresolved CXB spectra (CDFN-VF, CDFN-F, and CDFS) in the 0.4–10 keV band are fit well by a simple model consisting of a power law absorbed by the Galactic hydrogen column ( $N_H = 1.5 \times 10^{20} \text{ cm}^2$  for CDFN and  $0.9 \times 10^{20} \text{ cm}^2$  for CDFS) representing the extragalactic component, plus unabsorbed local warm thermal emission with solar heavy element abundances (the APEC model [65]). We assumed the power law to be the same between the CDFN-VF and CDFN-F spectra, but allowed it to be different for CDFS, since it points to a different region of the sky. Thermal models were allowed to be different between all three datasets, because they may also include a time-variable near-Earth charge exchange contribution (the dominant features of both the thermal and charge-exchange components is an OVII line around 570 eV, so they are difficult to disentangle).

The resulting fits are shown in Fig. 1. All three spectra are fit well, with a total reduced  $\chi^2$  of 0.87; no residual linelike features are seen. We can place an upper limit on such a line as a function of energy, excluding the range  $E < 0.8$  keV, where such a limit would not be interesting because of strong emission lines in the Galactic thermal spectrum, not resolved well by the ACIS CCD. To do this, we added a monochromatic line to the spectral model with the relative normalizations between the CDF regions de-

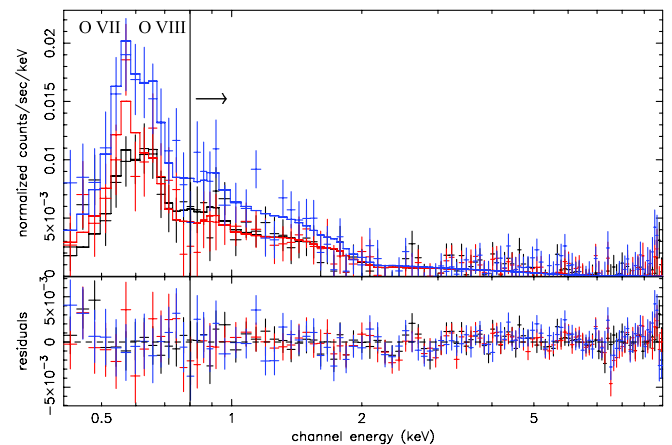


FIG. 1 (color online). The three unresolved CXB spectra [CDFN-VF (black), CDFN-F (red), and CDFS (blue)] in the 0.4–10 keV band. They are fit well by a simple model consisting of a power law absorbed by the Galactic hydrogen column representing the extragalactic component, plus unabsorbed local warm thermal emission. All three spectra are fit well, with a total reduced  $\chi^2$  of 0.87, and no residual linelike features are seen. Only energies  $E > 0.8$  keV are used for the line flux limits. See text for details.

terminated from the predicted neutrino brightness in the directions of those fields (Sec. II) and the region solid angles. For both the low-mass and high-mass Galaxy models, this ratio for CDFS/CDFN is 1.14. For each line energy in the range 0.8–9 keV, we refit the model and derived upper limits on the neutrino line normalization, allowing all other model parameters to vary as above (so that the neutrino line was allowed to account for the flux from other model components).

The spectra were binned in such a way that an emission line would be resolved at all energies and the statistics in each bin is Gaussian. The upper limits on the line normalization can then be derived from  $\Delta\chi^2$  w.r.t. the best-fit model. It is an adequate estimate (cf. Ref. [66]), because the sky signal is a small fraction of the underlying detector background count rate (20% and 3% in the 1–2 and 2–8 keV bands, respectively), which dominates the statistics. We note that while the CDF spectra are statistically independent, the detector background spectrum is almost the same for all three datasets, which introduces correlations among the three resulting CXB spectra. This has been taken into account by a simple Monte-Carlo simulation, from which we determined that for our particular combination of the CDF and background exposures,  $2\sigma$  and  $3\sigma$  upper limits for one interesting parameter correspond to  $\Delta\chi^2$  of 8.8 and 19.7, respectively, (compared to 4 and 9 for uncorrelated spectra). Using these values, we obtained

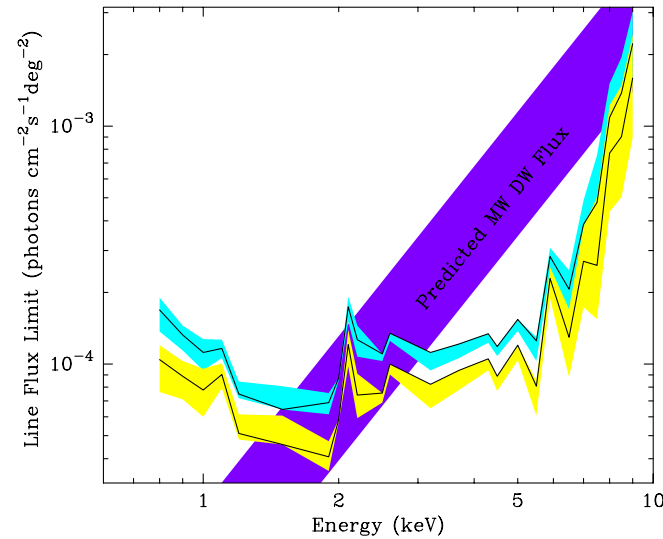


FIG. 2 (color online). Shown are the limits on the flux in a line as a function of energy from the CDFN-VF, CDFN-F, and CDFS. For each line energy in the range 0.8–9 keV, all model parameters were allowed to vary while deriving upper limits on the sterile neutrino line normalization. The upper line and (cyan) band are the  $3\sigma$  limit, with the band representing uncertainty in the detector background modeling. The lower band and line correspond to that from the  $2\sigma$  limits. The diagonal band is the range of expected line flux from the MW halo as a function of energy for the sterile neutrino in a DW production model.

upper limits on the neutrino line flux shown in Fig. 2. The constraints generally follow the energy dependence of the ACIS effective area and the presence of bright background lines (e.g., the fluorescent Au line at  $E = 2.1$  keV). In addition, we varied the normalization of the detector background spectrum by  $\pm 3\%$  (simultaneously for all three spectra), which represents the background modeling uncertainty (H06). The effect of this is shown as bands around the  $2$  and  $3\sigma$  limits in Fig. 2. We use the upper envelopes of these bands for the constraints below. The parameter space excluded by these constraints are shown, relative to other constraints, in Fig. 3.

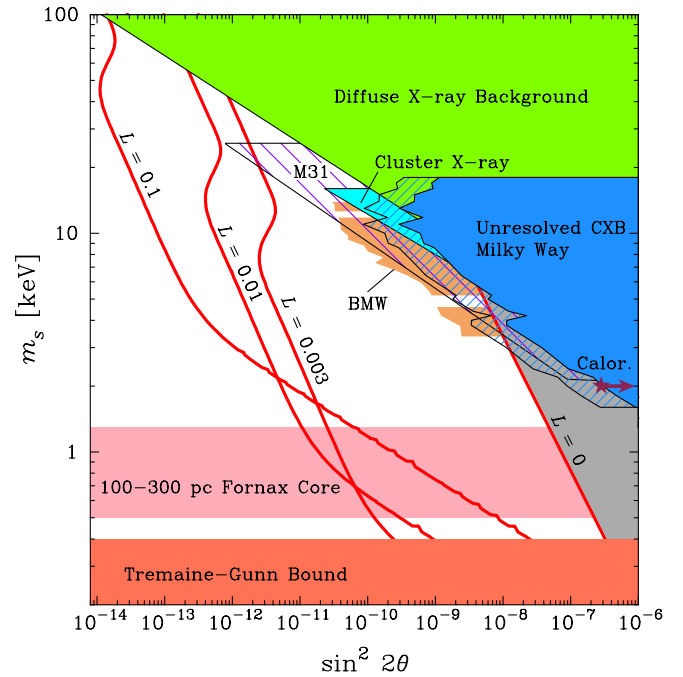


FIG. 3 (color online). Full parameter space constraints for the sterile neutrino production models, assuming sterile neutrinos constitute the dark matter. Contours labeled with lepton number  $L = 0$ ,  $L = 0.003$ ,  $L = 0.01$ ,  $L = 0.1$  are production predictions for constant comoving density of  $\Omega_s = 0.24$  for  $L = 0$ , and  $\Omega_s = 0.3$  for nonzero  $L$  [29]. Constraints from the CXB with the minimal MW halo model are in the solid (blue) region, while the maximal MW halo model excludes the adjacent diagonally hatched region. Also shown are exclusion regions from the diffuse X-ray background (green) [67], from XMM-Newton observations of the Coma and Virgo clusters (light blue) [68], observations of Andromeda (M31) in wide hatching [40], and limits from the MW by Boyarsky *et al.* [41] (BMW). The region at  $m_s < 0.4$  keV is ruled out by a conservative application of the Tremaine–Gunn bound [10]. The gray region to the right of the  $L = 0$  case is where sterile neutrino dark matter is over-produced. The constraint from the MW calorimeter soft X-ray background observation is the star and arrow, marked “Calor.” Also shown is the horizontal band of the mass scale consistent with producing a 100–300 pc core in the Fornax dwarf galaxy [5]. The nonresonant and resonant production curves come from Refs. [28,29], respectively.

In the DW model, these upper limits correspond to  $2\sigma$  limits on the sterile neutrino particle mass

$$m_s < \begin{cases} 2.87 \text{ keV} & (\text{high mass MW}) \\ 5.66 \text{ keV} & (\text{low mass MW}). \end{cases} \quad (8)$$

As is clear from these limits, there is considerable uncertainty due to the modeling of the dynamics of the MW halo.

#### IV. OBSERVATIONS OF THE SOFT X-RAY BACKGROUND

Here we explore the constraints from a related observation at  $E < 1$  keV using a detector with a much higher spectral resolution. The observation was made with an X-ray calorimeter flown on a sounding rocket, as reported by McCammon *et al.* [54]. The spectrum from their 100 s exposure is shown in the upper panel of Fig. 4. The observation was made towards Galactic coordinates  $\ell = 90^\circ$ ,  $b = +60^\circ$ . The mass surface density averaged over the wide ( $\Omega = 0.81$  sr) field of view of this experiment is

$$\bar{S}_{\text{dm}} = \begin{cases} 0.0460 \text{ g cm}^{-2} & (\text{high mass MW}) \\ 0.0138 \text{ g cm}^{-2} & (\text{low mass MW}). \end{cases} \quad (9)$$

The quantity  $\Omega \bar{S}_{\text{dm}}$ , which determines the expected sterile neutrino decay signal in the spectrum, is  $2.5 \times 10^5$  times higher than in the CDF observations. The dwarf spheroidal galaxies Ursa Minor and Draco lie within the FOV of this observation, but contribute only 2% to  $\bar{S}_{\text{dm}}$ .

To get a rough idea of how sensitive this experiment is to the sterile neutrino decay, we estimated the neutrino line

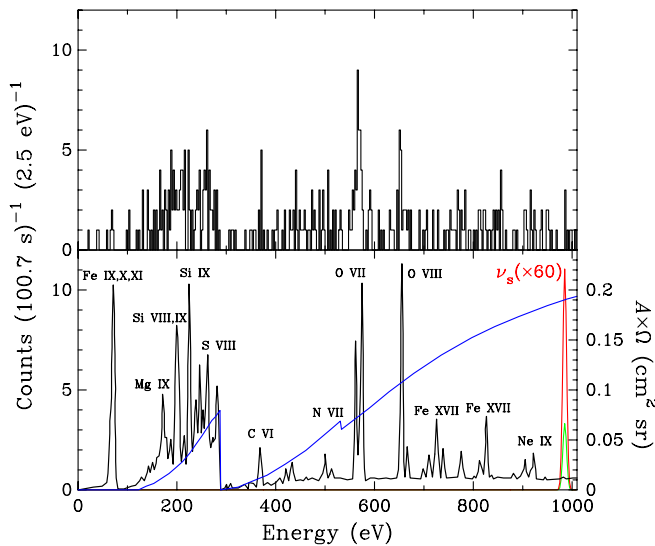


FIG. 4 (color online). The upper panel is the spectrum soft X-ray background as measured by McCammon *et al.* [54]. The lower panel shows the atomic line model, detector response function (blue) and expected contribution ( $\times 60$ ) due to sterile neutrino decay of the DW production model with the minimal (lower, green) and maximal (upper, red) MW halo models.

flux at  $E = 1$  keV. Using the detector response and exposure time from McCammon *et al.*, we find that an emission line from the  $m_s = 2$  keV sterile neutrino in the DW model would contain 1.8 or 0.5 counts in our maximum and minimum halo mass models, respectively. This is obviously too low to be detectable in the present data. A rough upper limit on the line flux at  $E = 1$  keV can be derived in the following way. The observed background in the McCammon spectrum at 1 keV is  $\sim 1.5$  counts per 2.5 eV bin, so  $\sim 5$  counts within FWHM of 9 eV. For Poissonian statistics, for an emission line on top of this background, a  $3\sigma$  upper limit is  $\sim 12$  counts (9 counts within the FWHM), or  $2\sigma$  limit of 6 counts. This would place a  $2\sigma$  limit between 3 and 11 times the mixing angle  $\sin^2 2\theta$  predicted by the DW model, for the high and low-mass MW models, respectively, at a sterile neutrino particle mass of 2 keV. For the low-mass case, this corresponds to excluding mixing angles at  $\sin^2 2\theta \gtrsim 3 \times 10^{-7}$  (see Fig. 3). At lower energies the detector efficiency and the neutrino decay rate both decline, so the constraints weaken rapidly. Nevertheless, the above limit for  $m_s = 2$  keV is similar to our ACIS constraints from a much longer observation, which shows the huge benefit of a wide FOV combined with a calorimetric energy resolution.

#### V. DISCUSSION AND CONCLUSIONS

The measurement by Hickox and Markevitch [52,53] of the unresolved cosmic X-ray background, produced by a total of 3 Ms observations by the ACIS CCD aboard the *Chandra* X-ray telescope, presents a constraint on the presence of a line flux that would be expected due to the decay of the sterile neutrino dark matter candidate comprising the dark matter halo of the MW. We find that the  $2\sigma$  upper limits on the sterile neutrino particle mass in the simplest (DW) production mechanism are in the range of  $m_s < 2.9$  and  $m_s < 5.7$  keV for high and low-mass estimates of the MW dark matter halo, respectively. To be conservative, the higher value for the upper limit of 5.7 keV is the robust 95% CL upper limit to conclude from the CXB analysis in the work presented here. More accurate dynamical measures of the MW halo are directly relevant for the particle-mass constraints presented here. In addition, we find that there is a significant limit to potential constraints from the *Chandra* observatory at photon energies  $E_\gamma \lesssim 1$  keV due to the presence of emission lines of the low temperature gas in the MW as well as the rapidly worsening relative energy resolution of the ACIS (as well as XMM EPIC) detector at these energies. This limits potential constraints from *Chandra* (or *XMM-Newton*) on the sterile neutrino particle mass to not better than  $m_s \approx 2$  keV.

The limits presented here from the MW contribution to the measured CXB in *Chandra* are comparable to that from the *XMM-Newton* observation of Andromeda,  $m_s < 3.5$  keV (95% CL) for the DW model, by Watson *et al.*

[40] who use a stringent requirement of the decay signal to be 4 times the astrophysical background within a bin to place this upper limit. Their constraints in the full parameter space (Fig. 3) were derived using an energy-averaged flux-to-counts conversion instead of the direct spectral fitting, which resulted in an approximate power-law constraint. In reality, their constraints must weaken at high energies as they do in this work, because the *XMM-Newton* effective area also declines sharply with energy.

The MW constraints by Boyarsky *et al.* [39] from the *XMM-Newton* X-ray background data in the full parameter space are comparable to ours. Their more recent analysis of the XMM background data [41] resulted in  $3\sigma$  constraints plotted in Fig. 3 (where the horizontal gaps correspond to the intervals  $E = 2.3\text{--}2.6$  keV and  $5.9\text{--}6.3$  keV excluded from their spectral fits). Their adopted MW halo model lies between our minimum and maximum mass models. While *Chandra* has an advantage over *XMM-Newton* of a more stable instrumental background and almost complete removal of the CXB in our deep exposures, the solid angle subtended by the *XMM-Newton* FOV is about 10 times greater than ours. This results in a proportionally higher expected MW sterile neutrino signal and more stringent constraints. On the other hand, because of the above two reasons, we could afford to derive constraints in a slightly wider energy range.

Reimer-Sorenson *et al.* [42] also analyzed *Chandra* CXB observations using the blank-sky data, and derived constraints on the MW sterile neutrino flux. Because they did not remove the ACIS internal background (that dominates at all energies and is well calibrated), their constraints on the flux are about 2 orders of magnitude weaker than ours.

We have also analyzed a related observation by McCammon *et al.* [54] in the soft X-ray, motivated by the high spectral resolution of the observation at low

photon energies, as well as the large field of view (0.81 ster) providing a corresponding 2 orders of magnitude larger MW halo mass in the field of view compared to the CDF observations. We find that though this observation in itself does not provide competitive constraints in the DW production model, longer exposure observations with low backgrounds may detect or place constraints within a photon energy range ( $E_\gamma < 1$  keV) and particle-mass range ( $m_s < 2$  keV), which is inaccessible to current X-ray telescopes. This observation constrains  $m_s = 2$  keV neutrinos to not have  $\sin^2 2\theta \gtrsim 3 \times 10^{-7}$ . Although this region is excluded in the DW model due to overproduction, the constraint may be of interest for low reheating temperature or dilution production models [32,33]. Future observations of the type by McCammon *et al.* in the soft X-ray, as well as those possible with the *Constellation-X* observatory at higher photon energies [35], may probe the full parameter space for oscillation-based sterile neutrino dark matter production models.

## ACKNOWLEDGMENTS

We would like to thank John Beacom, Daniel Boyanovsky, A. Boyarsky, Georg Raffelt, Oleg Ruchayskiy and Louie Strigari for useful discussions. K.N.A. would like to thank the Harvard-Smithsonian Center for Astrophysics for hospitality, where initial work on this project took place, and the Max Planck Institute for Physics in Munich for hospitality, where it was completed. M.M. was supported by NASA contract No. NAS8-39073 and *Chandra* grant No. GO4-5152X. Work performed at LANL was carried out under the auspices of the NNSA of the U. S. Department of Energy at Los Alamos National Laboratory under Contract No. DE-AC52-06NA25396.

- 
- [1] D.N. Spergel *et al.*, astro-ph/0603449 [Astrophys. J. (unpublished)].
  - [2] M. Tegmark *et al.*, Phys. Rev. D **74**, 123507 (2006).
  - [3] T. Goerdt, B. Moore, J.I. Read, J. Stadel, and M. Zemp, Mon. Not. R. Astron. Soc. **368**, 1073 (2006).
  - [4] F.J. Sanchez-Salcedo, J. Reyes-Iturbide, and X. Hernandez, Mon. Not. R. Astron. Soc. **370**, 1829 (2006).
  - [5] L.E. Strigari *et al.*, Astrophys. J. **652**, 306 (2006).
  - [6] G. Gilmore *et al.*, astro-ph/0608528.
  - [7] A.A. Klypin, A.V. Kravtsov, O. Valenzuela, and F. Prada, Astrophys. J. **522**, 82 (1999).
  - [8] B. Moore *et al.*, Astrophys. J. **524**, L19 (1999).
  - [9] G.R. Blumenthal, H. Pagels, and J.R. Primack, Nature (London) **299**, 37 (1982).
  - [10] P. Bode, J.P. Ostriker, and N. Turok, Astrophys. J. **556**, 93 (2001).
  - [11] M. Kaplinghat, Phys. Rev. D **72**, 063510 (2005).
  - [12] J.A.R. Cembranos, J.L. Feng, A. Rajaraman, and F. Takayama, Phys. Rev. Lett. **95**, 181301 (2005).
  - [13] W. Hu, R. Barkana, and A. Gruzinov, Phys. Rev. Lett. **85**, 1158 (2000).
  - [14] L.E. Strigari, M. Kaplinghat, and J.S. Bullock, astro-ph/0606281.
  - [15] Z.G. Berezhiani and R.N. Mohapatra, Phys. Rev. D **52**, 6607 (1995).
  - [16] E.J. Chun and H.B. Kim, Phys. Rev. D **60**, 095006 (1999).
  - [17] P. Langacker, Phys. Rev. D **58**, 093017 (1998).

- [18] N. Arkani-Hamed, S. Dimopoulos, G.R. Dvali, and J. March-Russell, *Phys. Rev. D* **65**, 024032 (2001).
- [19] K. Abazajian, G. M. Fuller, and M. Patel, *Phys. Rev. Lett.* **90**, 061301 (2003).
- [20] T. Asaka, S. Blanchet, and M. Shaposhnikov, *Phys. Lett. B* **631**, 151 (2005).
- [21] A. Kusenko and G. Segre, *Phys. Rev. D* **59**, 061302 (1999).
- [22] G.M. Fuller, A. Kusenko, I. Mocioiu, and S. Pascoli, *Phys. Rev. D* **68**, 103002 (2003).
- [23] A. Kusenko, *Int. J. Mod. Phys. D* **13**, 2065 (2004).
- [24] J. Hidaka and G.M. Fuller, *Phys. Rev. D* **74**, 125015 (2006).
- [25] P.L. Biermann and A. Kusenko, *Phys. Rev. Lett.* **96**, 091301 (2006).
- [26] S. Dodelson and L.M. Widrow, *Phys. Rev. Lett.* **72**, 17 (1994).
- [27] X.-d. Shi and G.M. Fuller, *Phys. Rev. Lett.* **82**, 2832 (1999).
- [28] K. Abazajian, *Phys. Rev. D* **73**, 063506 (2006).
- [29] K.N. Abazajian and G.M. Fuller, *Phys. Rev. D* **66**, 023526 (2002).
- [30] K. Abazajian, G. M. Fuller, and M. Patel, *Phys. Rev. D* **64**, 023501 (2001).
- [31] M. Shaposhnikov and I. Tkachev, *Phys. Lett. B* **639**, 414 (2006).
- [32] T. Asaka, A. Kusenko, and M. Shaposhnikov, *Phys. Lett. B* **638**, 401 (2006).
- [33] G. Gelmini, S. Palomares-Ruiz, and S. Pascoli, *Phys. Rev. Lett.* **93**, 081302 (2004).
- [34] K. Abazajian and S.M. Koushiappas, *Phys. Rev. D* **74**, 023527 (2006).
- [35] K. Abazajian, G. M. Fuller, and W.H. Tucker, *Astrophys. J.* **562**, 593 (2001).
- [36] A.D. Dolgov and S.H. Hansen, *Astropart. Phys.* **16**, 339 (2002).
- [37] M. Drees and D. Wright, hep-ph/0006274.
- [38] P.B. Pal and L. Wolfenstein, *Phys. Rev. D* **25**, 766 (1982).
- [39] A. Boyarsky, A. Neronov, O. Ruchayskiy, M. Shaposhnikov, and I. Tkachev, astro-ph/0603660.
- [40] C.R. Watson, J.F. Beacom, H. Yuksel, and T.P. Walker, *Phys. Rev. D* **74**, 033009 (2006).
- [41] A. Boyarsky, J. Nevalainen, and O. Ruchayskiy, astro-ph/0610961.
- [42] S. Riemer-Sorensen, S.H. Hansen, and K. Pedersen, *Astrophys. J.* **644**, L33 (2006).
- [43] P. McDonald *et al.*, *Astrophys. J. Suppl. Ser.* **163**, 80 (2006).
- [44] U. Seljak, A. Makarov, P. McDonald, and H. Trac, *Phys. Rev. Lett.* **97**, 191303 (2006).
- [45] M. Viel, J. Lesgourgues, M. G. Haehnelt, S. Matarrese, and A. Riotto, *Phys. Rev. Lett.* **97**, 071301 (2006).
- [46] M. Viel, J. Lesgourgues, M. G. Haehnelt, S. Matarrese, and A. Riotto, *Phys. Rev. D* **71**, 063534 (2005).
- [47] K. Abazajian, *Phys. Rev. D* **73**, 063534 (2006).
- [48] U. Seljak, A. Slosar, and P. McDonald, *J. Cosmol. Astropart. Phys.* **10** (2006) 014.
- [49] G. Mangano *et al.*, *Nucl. Phys.* **B729**, 221 (2005).
- [50] R.H. Cyburt, B.D. Fields, K.A. Olive, and E. Skillman, *Astropart. Phys.* **23**, 313 (2005).
- [51] L. Hui *et al.* (unpublished).
- [52] R. C. Hickox and M. Markevitch, *Astrophys. J.* **645**, 95 (2006).
- [53] R. C. Hickox and M. Markevitch (unpublished).
- [54] D. McCammon *et al.*, *Astrophys. J.* **576**, 188 (2002).
- [55] V.D. Barger, R. J. N. Phillips, and S. Sarkar, *Phys. Lett. B* **352**, 365 (1995).
- [56] T. Asaka, M. Laine, and M. Shaposhnikov, *J. High Energy Phys.* **01** (2007) 091.
- [57] A. Klypin, H. Zhao, and R. S. Somerville, *Astrophys. J.* **573**, 597 (2002).
- [58] G. Battaglia *et al.*, *Mon. Not. R. Astron. Soc.* **364**, 433 (2005).
- [59] L.M. Widrow and J. Dubinski, *Astrophys. J.* **631**, 838 (2005).
- [60] J.F. Navarro, C. S. Frenk, and S. D. M. White, *Astrophys. J.* **462**, 563 (1996).
- [61] V. Avila-Reese, P. Colín, O. Valenzuela, E. D’Onghia, and C. Firmani, *Astrophys. J.* **559**, 516 (2001).
- [62] M. C. Weisskopf *et al.*, *Publ. Astron. Soc. Pac.* **114**, 1 (2002).
- [63] W.N. Brandt *et al.*, *Astron. J.* **122**, 1 (2001).
- [64] R. Giacconi *et al.*, *Astrophys. J. Suppl. Ser.* **139**, 369 (2002).
- [65] R. K. Smith, N. S. Brickhouse, D. A. Liedahl, and J. C. Raymond, *Astrophys. J.* **556**, L91 (2001).
- [66] R. Protasov, D. A. van Dyk, A. Connors, V.L. Kashyap, and A. Siemiginowska, *Astrophys. J.* **571**, 545 (2002).
- [67] A. Boyarsky, A. Neronov, O. Ruchayskiy, and M. Shaposhnikov, *Mon. Not. R. Astron. Soc.* **370**, 213 (2006).
- [68] A. Boyarsky, A. Neronov, O. Ruchayskiy, and M. Shaposhnikov, *Phys. Rev. D* **74**, 103506 (2006).